Journal of Materials Chemistry A

Accepted Manuscript

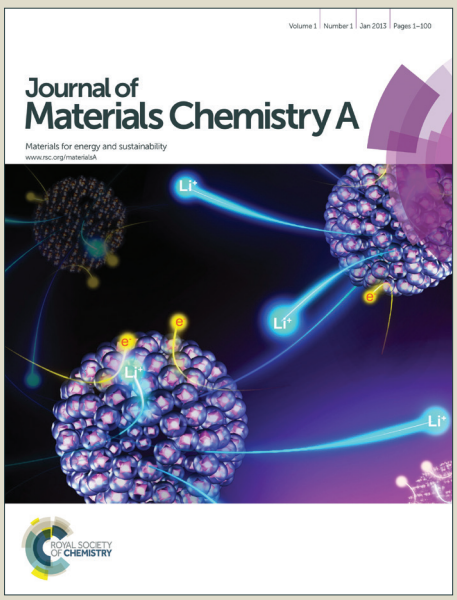

ROYAL SOCIETY OF CHEMISTRY

www.rsc.org/materialsA

Cite this: DOI: 10.1039/c0xx00000x

www.rsc.org/xxxxxx

ARTICLE TYPE

Synthesis of Novel Nitrogen-doped Lithium Titanate with Ultra-High Rate Capability Using Melamine as A Solid Nitrogen Source

Min Guo[a], Suqing Wang[a]*, Liang-Xin Ding[a], Long Zheng[a], and Haihui Wang[a,b]*

Received (in XXX, XXX) XthXXXXXXXXX 20XX, Accepted Xth XXXXXXXXX 20XX

DOI: 10.1039/b000000x

Nitrogen-doped $Li_4Ti_5O_{12}$ (LTO) is first synthesized by thermal decomposition of LTO and melamine. As indicated by TG, XPS and TEM analysis, the nitrogen is successfully doped in LTO, the generated TiN layer is deposited on the surface of the LTO particle. The LTO with certain nitrogen modification (LTON12) on the surface exhibits enhanced electronic conductivity and Li ion diffusivity. The LTON12 electrode exhibits much better rate capability and cycling performance than the pristine LTO. The LTON12 electrode delivers a capacity of 124.2 mAh g^{-1} after 500 cycles at 5C with a high capacity retention of 89.1% while the capacity retention of the pristine LTO is only 43.7%. In addition, the LTON12 exhibits a capacity of 74.3 mAh g^{-1} at even 100C with a fixed discharge rate of 1C. The excellent electrochemical performance of N-doped LTO is attributed to the improved electronic and ion conductivities provided by the thin TiN coating layer on the particle surface.

INTRODUCTION

With growing concerns over environmental issues and traditional energies including coal, oil and natural gas, developing renewable energy storage systems are urgently required.[1] Lithium ion batteries (LIBs) are under the spotlight for both the academic community and industry as a power source for hybrid electric vehicles (HEVs) to save petrified energy sources and decrease the environmental burden because of its safety, long cycle life, high energy density and friendliness to the environment.[2-5]

As an alternative to current carbon-based anodes, $Li_4Ti_5O_{12}$ (LTO) with its intrinsic characteristics shows promising electrochemical properties. On one hand, it possesses a relatively high potential plateau (around 1.5V versus Li^+/Li) to ensure safety of the battery by avoiding Li-metal deposition and the formation of solid electrolyte interface (SEI) layer on the surface of the electrode. On the other hand, LTO is a zero-strain insertion material, providing excellent lithium-ion mobility and long cycle life in the charge and discharge process.[6] Nevertheless, the commercial application of LTO in lithium-ion batteries is hindered by its kinetic problems of poor electronic conductivity (merely 10^{-13} S cm^{-1}) which leads to poor rate capability and serious electrochemical polarization at high current densities.

So far, tremendous research and development efforts have been reported to tackle this problem, including nanotechnology,[7-10] surface coating with an electron conductive layer[11-12] and structural doping with ions on Li, Ti or O sites of LTO.[13-16] Among these processes, a successful example is surface modification with nitrogen. Park made N-doped LTO by treating LTO in NH_3 (99.98 %) with the flow rate of 30 cm^3 min^{-1} for 10 minutes, introducing a mixed-valent intermediate phase and a conductive layer (TiN) on the surface of LTO, and the prepared N-doped LTO showed a significant enhanced performance.[17] Park et al. and Zhang et al. prepared the LTO particles by introducing a conductive TiN layer with heat treatment in NH_3 amorsphere.[18-19] Shao et al. also reported N-doped and TiN modified LTO with improved electrochemical performance.[20] Currently, the most used nitrogen source in those researches is gas source-ammonia. Unfortunately, NH_3 is dangerous, corrosive and environmentally unfriendly. On the other way, the nitrogen doping can be affected by the reaction time, the NH_3 concentration and the amount of LTO powders, which make it difficult to be controlled. As a result, it is infeasible to achieve large-scale production. Zhang et al. obtained LTO/TiN nanocomposites with improved rate and cyclic performances directly through ball-milling of LTO and TiN powders.[21] However, the final product is depended on the morphologies of the raw materials, and it is hard to get uniform coating of TiN on LTO particles without chemical reaction. Zhao et al. chose ionic liquid as a nitrogen source to synthesize N-doped LTO with excellent C-rate performance.[22] It is very easy to mix solid LTO with liquid very well and make uniform surface coating of TiN. However, the high price of the ionic liquid hinder its application in the industry. Considering the production cost and complexity, a facile and economical preparation route is required to facilitate practical application. The key is to find a suitable nitrogen source which is low cost, environmentally friendly and easily controlled in synthesize process.

Melamine ($C_3H_6N_6$) is a cheap industrial product with high nitrogen content (66.6 wt %). Our group have successfully synthesized N-doped graphene with high nitrogen content using melamine as a solid nitrogen sources.[23] Different from previous reported nitrogen doping methods with gas nitrogen source (NH_3) which is highly corrosive and environmentally unfriendly, we exploit a viable and scalable process to synthesize nitrogen-doped

LTO using thermal decomposition of the solid LTO and solid melamine in this work. The method is easier to be controlled and more suitable for mass production. Moreover, the whole preparation process is solid state reaction which is commonly used in industrial production.

EXPERIMENTAL SECTION

Synthesis and characterization

All of the reactants and solvents were of analytical grade and used without further purification. The pristine LTO was synthesized through traditional solid-state reaction. Typically, Li_2CO_3 and anatase TiO_2 powders with a molar ratio of Li:Ti=4.17:5 were first stirred by high-energy ball-milling (QM-3SP04) at a speed of 300 rpm for 10 hours to obtain the slurry. The slurry was dried at 80 °C and then grinded well. Then powder was further calcined at 850 °C for 12h with a heating rate of 2 °C min^{-1} in muffle furnace. Afterward, the obtained LTO and melamine were grinded thoroughly using a mortar and pestle at the weight ratio of 2:1, 1:1, 1:2, and then the mixture powders were calcined at 700 °C for 10h under Ar atmosphere to form N-doped lithium titanate, which were named LTON21, LTON11, LTON12, respectively.

The crystalline phases of the as-prepared materials were characterized by X-ray diffraction (XRD, Bruker D8 Advance) using Cu-Kα radiation (10°≤2θ≤80°) operated at 40.0 KV and 40 mA. The morphologies of the samples were observed using scanning electron microscopy (SEM, Nano430) and transmission electron microscopy (TEM) (FEI, Tecnai G2 F30 S-Twin). X-ray photoelectron spectroscopy (XPS) measurements were performed on a Perkin-Elmer PHI 550 system.

Electrochemical measurements

Electrochemical evaluation was carried out by assembling half-cell using lithium metal foil as the counter electrode. The working electrodes were formed by mixing active material powders with carbon black and polyvinylidene fluoride (PVDF) at a weight ratio of 75:15:10 in N-methyl-2-pyrrolidine (NMP), then the slurry was pasted on Cu foil and dried under vacuum at 80 °C for 12h. Afterward, the coin cells were assembled in an argon-filled glove box (Mikrouna, super 1220) where the oxygen and moisture contents were less than 1 ppm. Celgard 2325 microporous membrane was used as the separator. The electrolyte solution was 1 M $LiPF_6$ in EC/DEC (1:1, v/v). All the coin cells were cycled at different current densities between 1.0 and 2.5V using a battery testing system (Neware Electronic Co., China).

RESULTS AND DISCUSSION

Figure 1a shows XRD patterns of the bare LTO and the LTON12. All the strong diffraction peaks can be perfectly indexed for a cubic spinel structure with Fd-3m space group (JCPDS card No. 49-0207) which reveals that pure phase of LTO was successfully synthesized. No obvious change was observed in the XRD patterns of N-doped LTO powders (Figure S1). TG analysis in Figure 1b verifies the presence of nitrogen. There is no weight change in LTO sample, but in the case of LTON12, a weight increase of approximately 0.48% was observed, which might be due to the oxidation reaction of TiN to TiO_2.[24]

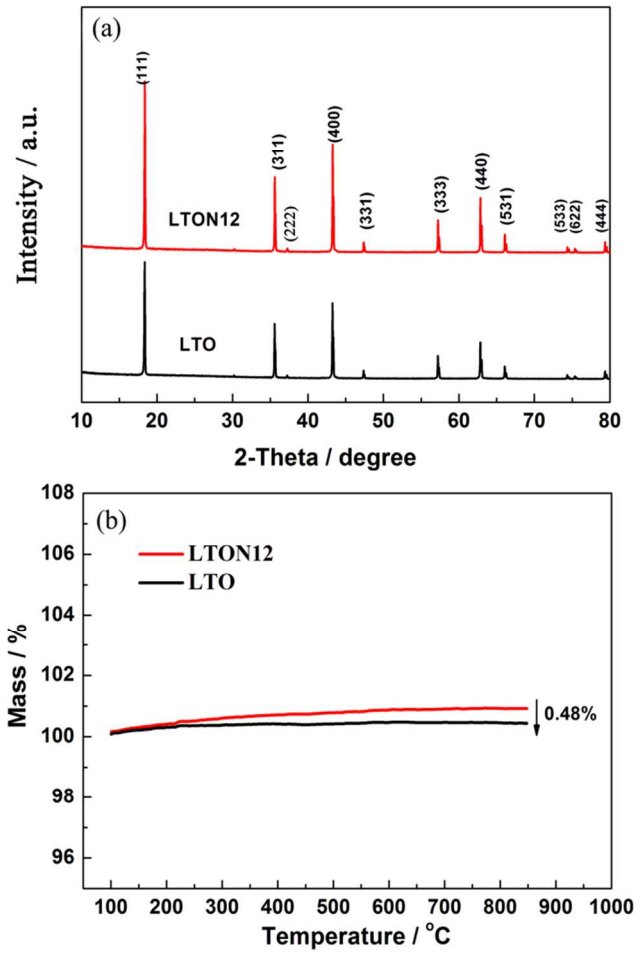

Figure 1. (a) X-ray diffraction patterns and (b) TG curves of the pristine LTO and LTON12.

Figure 2a-b show the morphologies of the pristine LTO and the LTON12. It is obvious that both samples are well crystallized and index as spinel $Li_4Ti_5O_{12}$. The particle size distributions are all ranging from 0.3 to 1.0 μm. Nitridation does not influence the structural and morphology of the LTO particles. The corresponding energy-dispersive X-ray (EDX) mapping images of Ti, O and N elements were employed (Figure S2). The distribution of N element is consistent with those of Ti and O, which implies that N element distributes uniformly in the particles.[22]

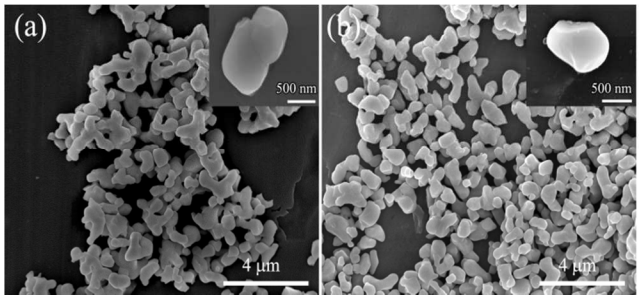

Figure 2. SEM images of the as-prepared samples: (a) LTO, (b) LTON12.

XPS was conducted to verify the existence of Ti^{3+}. As shown in Figure 3, typical doublet Ti2p peaks around at 464.2 eV and 458.5 eV appeared in the samples before and after N-doped

treatment, in consensus with characteristic peaks of Ti^{4+} in an octahedral environment. There is no obvious new peak for the sample LTON21 and LTON11, which might due to the low nitrogen doping in the particles (Figure S4). It is clear that a new Ti 2p doublet at lower binding energies (456.7 eV and 461.7 eV) is observed for the LTON12 sample which is assigned to the present of titanium nitride (Figure 3b).[25] The presence of Ti^{3+} in the LTON12 sample can lead to increase of electrons and eventually improve electronic conductivity. To further investigate the nitrogen content, elemental analysis is employed for LTON12 sample, the result shows that the nitrogen content is about 0.044 wt %. Raman spectra (Figure S5) of the pristine LTO and LTON12 were conducted. The Ti-O stretch vibration bands shifted from 665.9 cm^{-1} for LTO sample to 669.8 cm^{-1} for LTON12 powder due to the lower electrostatic negative force of N^{3-} than O^{2-}. Such shift could be well explained by the doping of nitrogen into $Li_4Ti_5O_{12}$.[20] It is demonstrated that the potential formation of titanium nitride thin films on the surface of LTO which may improve the electronic conductivity of the modified LTO due to the metal conductivity of TiN.

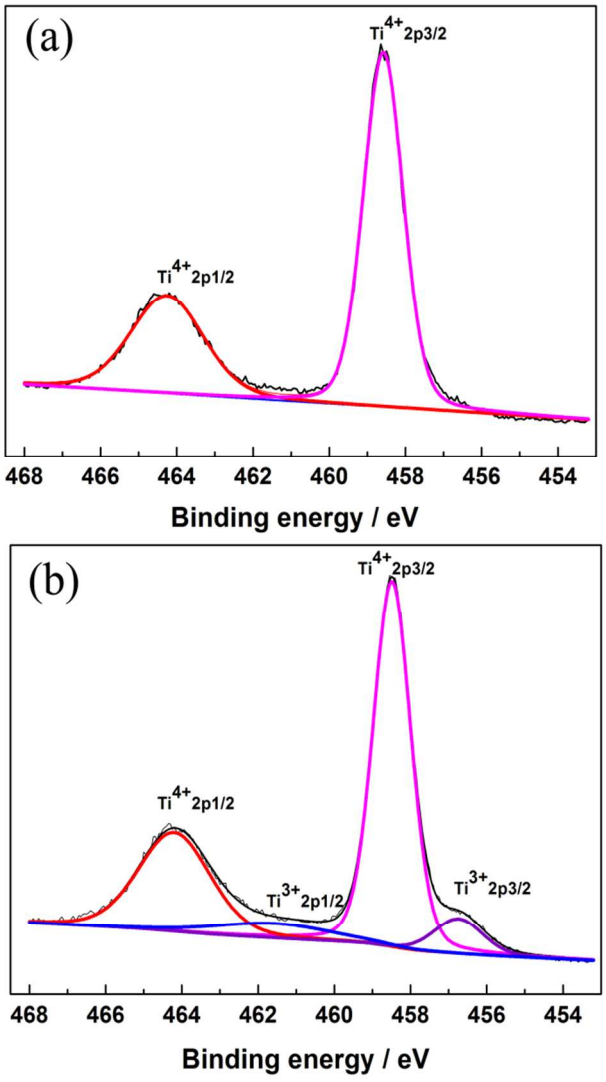

Figure 3. XPS spectrum of Ti 2p of (a) LTO, (b) LTON12.

The surface structure of the pristine LTO and the LTON12 powders were further clarified by TEM and HR-TEM, shown in Figure 4. Both samples show a very smooth surface, lattice spacing of 0.48 nm, corresponding to the (111) planes of the pristine LTO and the LTON12, and the selective area electron diffraction (SAED) patterns (insert of Figure 4c-d) indicate the high crystallization character of both two samples. It can be observed that a very thin uniform amorphous layer with a thickness of approximately 1.24 nm is formed on the surface, which is likely derived during the thermal decomposition of melamine. Shao et al. investigated the effect of TiN coating layer on the electrochemical performance of the LTO. If the thickness of TiN layer is too thick, it would block lithium ion transfer from the electrolyte to the electrode and then deteriorate the electrochemical performance.[20] And, several previous reports also indicated that LTO coating with thin TiN layer showed improved rate capability than pristine LTO due to the enhanced electronic conductivity.[20,21,24] Therefore, the as-prepared thin TiN layer (~1.24 nm) in our experiment might be beneficial to the electrochemical performance of $Li_4Ti_5O_{12}$.

To obtain the surface information of the particles, energy dispersive X-ray spectrometry (EDX) elemental scanning mappings of the LTON12 particle was further employed. Figure 5a shows the scanning path of the EDX test. The peak intensities shown in Figure 5b corresponding to the amount of Ti, O, and N elements, respectively. The result shows that the weight percentage of nitrogen element is 9.03% based on the total amount of the N, O and Ti elements (Table S1). The much higher nitrogen content detected by EDX elemental scanning mappings than the whole nitrogen percentage in the LTON12 is another evidence to prove that the N element is mostly distributed on the surface of the LTO particles.

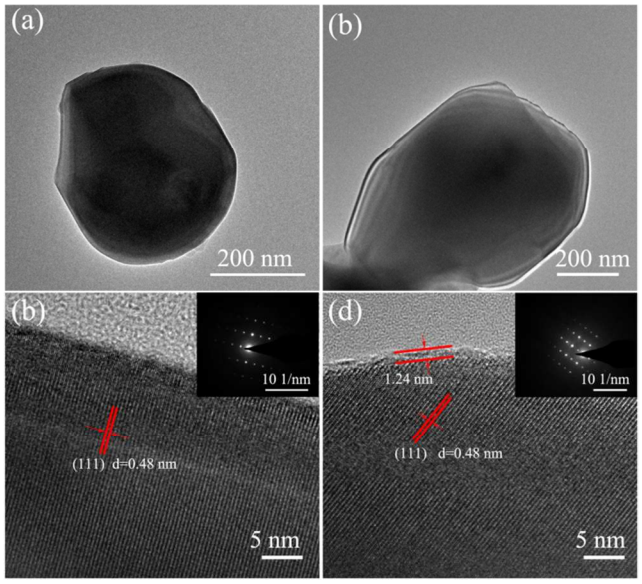

Figure 4. TEM images of the pristine LTO (a) and LTON12 (b); HRTEM image of the pristine LTO (c) and the LTON12 (d), insets are the corresponding selective area electron diffraction patterns.

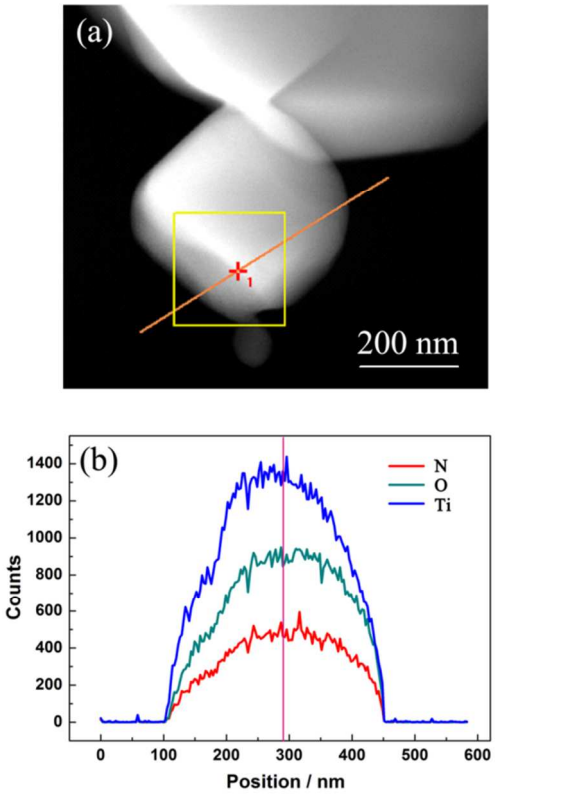

Figure 5. (a) STEM image, and (b) EDX elemental scanning mappings of LTON12.

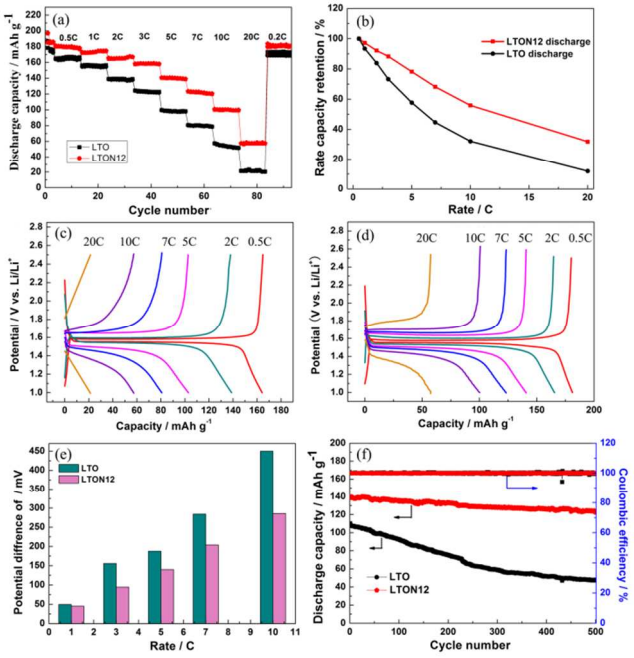

Figure 6. (a) Rate capabilities and (b) normalized capacity retentions of the pristine LTO and LTON12 under various current densities ranging from 0.2C to 20C; The voltage plateaus at different rates (0.5C, 2C, 5C, 7C, 10C, 20C) of (c) the pristine LTO and (d) the LTON12 electrodes; (e) Comparison of the charge/discharge plateau potential difference of the pristine LTO and LTON12 electrodes; (f) The long cycling performance and corresponding coulombic efficiency of the pristine LTO and the LTON12 electrodes at the rate of 5C.

Electrochemical performances of the pristine LTO and the LTON12 electrodes were evaluated over the potential window of 1.0-2.5V. Figure 6a shows the comparison of the rate performances of the pristine LTO and the LTON12 at various current densities. The discharge capacities show a significant decrease of the pristine LTO from 1C (1C=175 mA g^{-1}) to 20C, whereas the LTON12 decrease much more slowly at the same rates. This demonstrates a remarkably enhanced rate capability of LTO by N doping. At the high current rates, such as at 10C and 20C, the LTON12 delivers the capacities of 100.7 and 57.4 mAh g^{-1}, higher than the pristine LTO which merely exhibits 52.0 and 21.4 mAh g^{-1}, respectively. And, the discharge capacity of LTON12 at 10C is 55.9% of the capacity at 0.5C while the pristine LTO only delivers 32.1% of the discharge capacity at 0.5C (Figure 6b). The improved rate capabilities of the LTON12 is ascribed to the presence of Ti^{3+} after N doping enables faster electron transport which improves the electronic conductivities and rate performances. Figure 6c-d present the voltage profiles of LTO and LTON12 electrodes at the current rates from 0.5 C to 20 C. At a lower rate of 0.5C, both of the pristine LTO and the LTON12 show flat voltage plateaus at about 1.55V. As the current rate increases, it has no obvious plateau at 10C for the pristine LTO, while the plateau around at 1.78V can be easily observed even at 20C for the LTON12. The comparison of potential difference between the discharge and the charge plateaus at different rates is usually used to evaluate the polarization of the electrode. The values of potential difference are defined as the differences between the potentials of 50% fully charge and 50% fully discharge plateau.[25] As shown in Figure 6e, for the LTON12 electrode, the difference of voltage plateaus at 1C, 3C, 5C, 7C and 10C are 45.3, 94.6, 140.2, 204.0 and 286.0 mV, respectively. And the potential difference of the pristine LTO are 49.8 mV at 1C, 156.0 mV at 3C, 187.9 mV at 5C, 284.3 mV at 7C and 450.0 mV at 10C. It is obvious that the polarization of the LTON12 is significantly lower than that of the pristine LTO, which is attributed to the better reaction kinetics after N doping. Figure 6f shows the long-term cycling performances of the pristine LTO and the LTON12 at 5C. The initial capacity of the pristine LTO is 108.5 mAh g^{-1}, and it decreases to only 47.4 mAh g^{-1} after 500 cycles with a capacity retention of 43.7%. In the case of the LTON12, the discharge capacity is 139.5 mAh g^{-1} at first cycle and still maintains 124.2 mAh g^{-1} after 500 cycles with a capacity retention of 89.1%, which demonstrating a remarkable improved cyclic stability. Moreover, the coulombic efficiency for both samples are approximately 100% throughout the cycling, which mean that the lithium intercalation and release are well reversible.

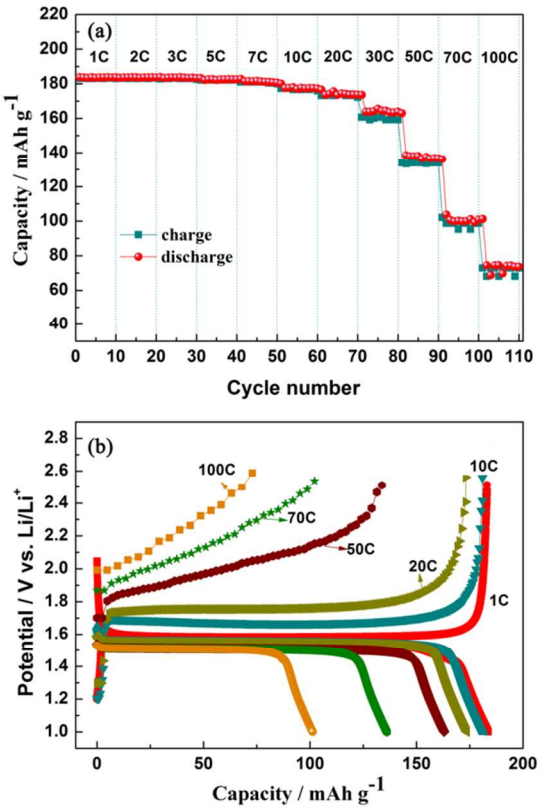

Figure 7. (a) Rate capability test and (b) the voltage profiles of the LTON12 at different rates (1C, 10C, 20C, 50C, 70C, 100C). The discharge rate is fixed at 1C.

In practical applications, lithium-ion batteries could be charged at a relatively low current density and discharged at high current densities. Correspondingly, the anode materials discharged at low current density and charged at high current density.[17,26] Meanwhile, currently commercial graphite anode in Li-ion cell cannot meet the power requirements of vehicles at start-up or speedup.[8, 27] It is meaningful to evaluate the charge capability of anode materials at high current rates. Before charged at each rate, the cell should be activated at low current density for three cycles. Figure 7a shows the capacity performance of a LTON12/Li cell at various charge rates with a fixed discharge rate of 1C (1C=175 mA g^{-1}). The initial capacity at 1C is 183.7 mAh g^{-1}. And it still remains 182.5mAh g^{-1} at 5C without obviously capacity fading. As the charge current increasing, the LTON12 shows excellent performance with high capacity retention. Even at 10 and 20C, the charge capacity is 177.5 and 173.8 mAh g^{-1}, which is 96.6% and 94.6% of the charge capacity observed at 1C. At extremely high charge current density of 100C, the charge capacity of LTON12 could still maintain 74.3 mAh g^{-1}. Figure 7b shows the voltage profiles at various charge rates with a fixed discharge rate at 1C. Due to the constant discharge rate, the discharge voltage plateau is kept at around 1.55V. Moreover, from 1C to 20C, the difference between the charge and discharge voltage plateau is small, which represents a fast kinetics of lithium insertion/extraction process. Even at 50C, 70C, and 100C (completely discharge in 55s, 29s and 15s), the LTON12 electrode exhibits obvious voltage plateaus. The results indicate that the LTON12 owns excellent reaction kinetics. N-doped LTO synthesized by thermal decomposition with melamine is a promising anode material in practical applications on high power devices.

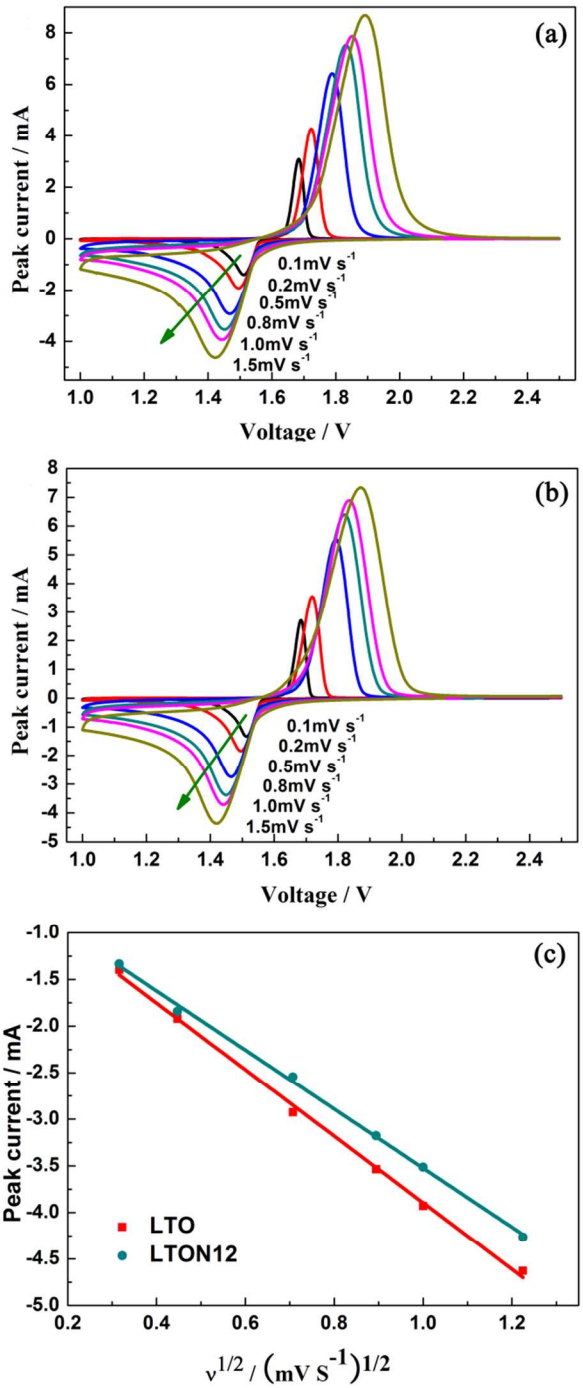

Figure 8. Cyclic voltammograms of (a) the pristine LTO, (b) LTON12; (c) Peak current against square root of scan rate for these two samples.

Figure 8a-b show the cyclic voltammograms (CV) of the pristine LTO and the LTON12 electrodes. All CV curves exhibit a pair of sharp peaks which is characteristic of electrochemical lithium insertion/extraction of $Li_4Ti_5O_{12}$. From Figure 8a-b, it could be observed that the potential window between redox peaks of the LTON12 electrode is similar with that of the pristine LTO at low scan rates (0.1 mV s^{-1}, 0.2 mV s^{-1} and 0.5 mV s^{-1}), and

smaller than that of the pristine LTO at higher scan rates (1.0 mV s^{-1} and 1.5 mV s^{-1}), which implies that the LTON12 electrode has a smaller potential polarization and better reaction kinetics than the pristine LTO at high current densities which is consistent with the above rate performances. Figure 8c shows the correlation between the anodic peak currents and the square roots of the scan rate for both electrodes, which matches the linear relationship very well. It is the typical behaviour of diffusion-controlled electrode reaction process.[28] The diffusion coefficient can be estimated based on the slop of the oblique line. Hence, it can be easily deduced that the N-doped LTO has the largest diffusion coefficient. Since both materials have almost the same particle size distribution, the increased diffusion coefficient of LTON12 should be attributed to the formation of conductive layer-TiN, which is beneficial to the quick migration of the inserted Li ion and increase the conductivity.

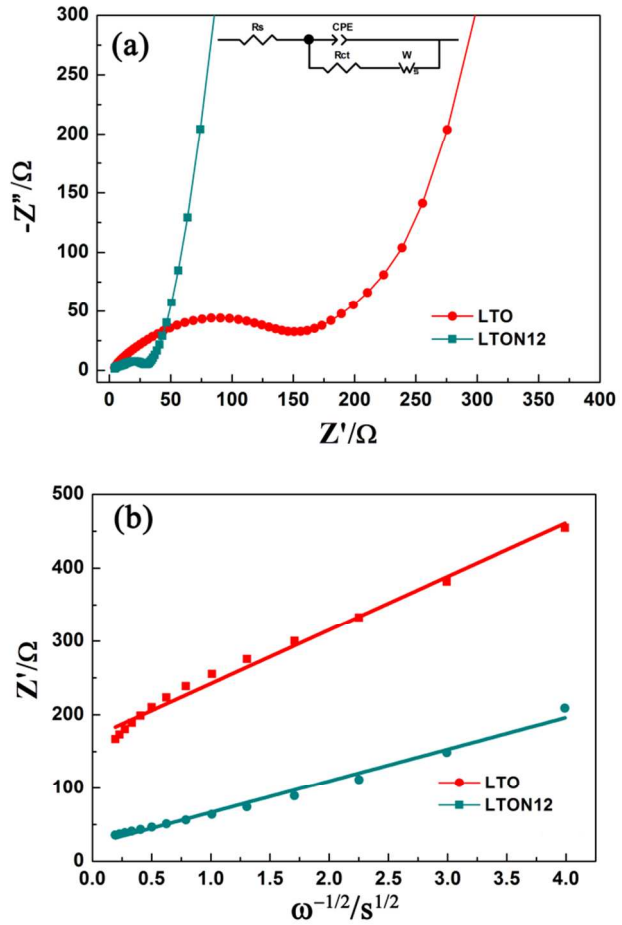

Figure 9. (a) Nyquist plots of the pristine LTO and the LTON12 samples; (b) The corresponding graph of Z' plotted against $\omega^{-1/2}$ at low frequency region.

In order to gain insight into the ultra-high rate performance of N-doped LTO, electrochemical impedance spectroscopy (EIS) was tested (Figure 9). Both EIS diagrams are composed of a depressed semicircle at high frequencies and an oblique linear Warburg part at low frequencies. The high frequency semicircle is related to the charge-transfer reaction and the low frequency indicates the Warburg impedance of long-range lithium-ion diffusion.[29] These impedance spectra were fitted by Zview software using an equivalent circuit mode, shown in the inset of the Figure 9a. Herein, R_s and R_{ct} are the solution resistance and charge transfer resistance at the particle/electrolyte interface, respectively. CPE represents the double-layer capacitance and passivation film capacitance. W represents the Warburg impedance. The parameters obtained by fitting are recorded in Table 1. It is obvious that the pristine LTO and LTON12 show similar R_s, but the LTON12 shows a much lower charge-transfer resistance (28.02 Ω) than that of the pristine LTO electrode (150.50 Ω), confirming that the nitrogen modification on the surface of the LTO particles improves the electrical conductivity.

Table 1. Impedance parameters derived from equivalent circuit model and lithium diffusion coefficient D_{Li+} for LTO and LTON12 electrodes.

Sample	R_s(Ω)	R_{ct}(Ω)	D_{Li+}(cm^2s^{-1})
LTO	2.45	150.50	7.77×10^{-12}
LTON12	2.76	28.02	2.71×10^{-10}

In addition, the EIS measurement has been considered as a useful method to calculate the chemical diffusion coefficient.[30] The Warburg impendence at low frequency corresponding to the diffusion of Li ions in the bulk of the electrode, has been used to determine the Li-ion diffusion coefficient.[31-34] The D_{Li+} for LTO can be calculated as the following equation:[35-36]

$$D_{Li} = \frac{1}{2}\left[\left(\frac{V_m}{AF\sigma_m}\right)\frac{dE}{dx}\right]^2 \qquad (1)$$

Where V_m is the molar volume of LTO (45.73 cm^3 mol^{-1}), F is the Faraday constant (96486 C mol^{-1}), A is the total contact area between the electrolyte and the electrode, dE/dx is the slope of the open-circuit voltage versus mobile Li^+ concentration x, and the σ_ω values at different voltages can be obtained from the slope of Z' vs. $\omega^{-1/2}$ in the Warburg region (Figure 9b), it can be summarized as

$$Z' = R + \sigma_w\omega^{-1/2} \qquad (2)$$

The calculated lithium diffusion coefficients (D_{Li+}) of the pristine LTO and LTON12 are shown in Table 1. D_{Li+} of LTON12 is 2.71×10^{-10} cm^2 s^{-1} which is two orders of magnitude higher than that of LTO (7.77×10^{-12} cm^2 s^{-1}). Obviously, the LTON12 has a bigger lithium diffusion coefficient, which indicates that the lithium ion mobility of LTO can be effectively improved by N doping. Consequently, the rate capability of the N-doped LTO can be improved substantially which is consistent with the electrochemical performance (Figure 6).

CONCLUSIONS

In conclusion, the N-doped LTO can be carried out successfully via the thermal decomposition of LTO particles mixed with melamine. Here, melamine is used as a solid nitrogen sources for nitridation process. As indicated by linear scanning EDX, homogenous TiN layer is in situ constructed on the surface of the primary LTO which is beneficial to the electronic conductivity. As a result, the N-doped LTO shows higher rate capability and better cycling stability than the pristine LTO. The improved electrochemical performance is due to the formation of TiN layer with moderate thickness on the surface of LTO which improves the electronic conductivity. The route of thermal decomposition of solid LTO and solid melamine is relatively simple, low cost

and controllable which has a great potential to apply in industrial production.

ACKNOWLEDGMENTS

The authors greatly acknowledge the financial support by National Science Fund for Distinguished Young Scholars of China (No. 21225625), Natural Science Foundation of China (No. 21306057), the Australian Research Council (ARC) through the Future Fellow Program (FT140100757), the Specialized Research Fund for the Doctoral Program of Higher Education (20120172120011), The Pearl River Scholar Program of Guangdong Province and Fundamental Research Funds for the Central Universities, SCUT.

NOTES

[a] *School of Chemistry & Chemical Engineering, South China University of Technology, Wushan Road, Guangzhou 510640, China. Fax/Tel: +86-20-87110131; E-mail: cesqwang@scut.edu.cn, hhwang@scut.edu.cn*
[b] *School of Chemical Engineering, The University of Adelaide, Adelaide, SA 5005, Australia*

† Electronic Supplementary Information (ESI) available: [XRD patterns, SEM images, XPS spectrum and rate capabilites of LTON21 and LTON11; EDX element distribution mapping of (b) Ti, (c) O, (d) N elements for LTON12 sample; Raman spectra of LTO and LTON12 powders; The quantification results of EDX elemental mapping.]. See DOI: 10.1039/b000000x/

REFERENCES

1 K. Kang, Y. S. Meng, J. Breger, C. P. Grey, G. Ceder, *Science*, 2006, **311**, 977-980.
2 L. Zhou, D. Y. Zhao, X. W. Lou, *Angew. Chem.*, 2012, **124**, 243-245.
3 H. G. Jung, M. W.Jang, J. Hassoun,Y. K. Sun, B.Bcrosati, *Nature Commun.*, 2011, **2**, 516.
4 H. B. Wu, J. S. Chen, H. H. Hng, X. W. Lou, *Nanoscale*, 2012, **4**, 2526-2542.
5 L. Li, Z. Wu, S. Yuan, X. B. Zhang, *Energy Environ. Sci.*, 2014, **7**, 2101-2122.
6 L. Yu, H. B. Wu, X. W. Lou, *Adv. Mater.*, 2013, **25**, 2296-2300.
7 M. Venkateswarlu, C. Chen, J. S. Do, C. W. Lin, T. C. Chou, B. J. Hwang, *J. Power Sources*, 2005, **146**, 204-208.
8 C. Jiang, M. Ichihara, I. Honma, H. S. Zhou, *Electrochim. Acta*, 2007, **52**, 6470-6475
9 D. Su, F. Wang, C. Ma, *Nano Energy*, 2013, **2**, 343-350.
10 G. N. Zhu, H. J. Liu, J. H. Zhang, C. X. Wang, Y. G. Wang, Y. Y. Xia, *Energy Environ. Sci.*, 2011, **4**, 4016-4022.
11 L. Cheng, J. Yan, G. N. Zhu, J. Y. Luo, C. X. Wang, Y. Y. Xia, *J. Mater. Chem.*, 2010, **20**, 595-602.
12 X. Guo, H. F. Xiang, T. P. Zhou, W. H. Li, X. W. Wang, J. X. Zhou, Y.Yu, *Electrochim. Acta*, 2013, **109**, 33-38.
13 B. B. Tian, H. F. Xiang, L. Zhang, Z. Li, H. H. Wang, *Electrochim. Acta*, 2010, **22**, 5453-5458.
14 M. Ji, Y. L. Xu, Z. Zhao, H. Zhang, D. Liu, C. J. Zhao, X. Z. Qian, C. H. Zhao, *J. Power Sources*, 2014, **263**, 296-303.
15 C. C. Li, Q. H. Li, L. B. Chen, T. H. Wang, *ACS Appl. Mater. Interface* 2012, **4**, 1233-1238.
16 B. F. Wang, J. S. Wang, J. Cao, H. H. Ge, Y. F. Tang, *J. Power Sources*, 2014, **266**, 150-154.
17 K. S. Park, A. Benayad, D. J. Kang, S. G. Doo, J. Am. Chem. Soc., 2008, **130**, 14930-14931.
18 H. Park, T. Song, H. Han, U. Paik, *J. Power Sources*, 2013, **244**, 726-730.
19 H. Q. Zhang, Q. J. Deng, C. X. Mou, Z. L. Huang, Y. Wang, A. J. Zhou, *J. Power Sources*, 2013, **239**, 538-545.
20 Z. N. Wan, R. Cai, S. M. Jiang, Z. P. Shao, *J. Mater. Chem.*, 2012, **22**, 17773-17781.
21 J. W. Zhang, W. Cai, F. L. Zhang, L. G. Yu, Z. S. Wu, Z. J. Zhang, *J. Power Sources*, 2012, **211**, 133-139.
22 L. Zhao, Y. S. Hu, H. Li, Z. X. Wang, L. Q. Chen, *Adv. Mater.*, 2011, **23**, 1385-1388.
23 D. D. Cai, S. Q. Wang, P. C. Lian, X. F. Zhu, D. D. Li, W. S. Yang, H. H. Wang, *Electrochim. Acta*, 2013, **90**, 492-497.
24 X. Li, H. C. Lin, W. J. Cui, Q. Xiao, J. B. Zhao, *ACS Appl. Mater. Interface*, 2014, **6**, 7895-7901.
25 J. Q. Wang, Z. Z. Yang, W. H. Li, X. H. Zhong, L. Gu, Y. Yu, *J. Power Sources*, 2014, **266**, 323-331.
26 D. Wang, N. Ding, X. H. Song, C. H. Chen, *J. Mater. Sci.*, 2009, **44**, 198-203.
27 X. Y. Feng, C. Shen, N. Ding, C. H. Chen, *J. Mater. Chem.*, 2012, **22**, 20861-20865.
28 J. X. Qiu, C. Lai, E. Gray, S. Li, S. Y. Qiu, E. Strounina, C. H. Sun, H. J. Zhao, S. Q. Zhang, *J. Mater. Chem. A*, 2014, **2**, 6353-6358.
29 J. X. Qiu, C. Lai, S. Li, S. Q. Zhang, *RSC Adv.*, 2014, **4**, 18899-18903.
30 Y. H. Rho, K. Kanamura, *J. Solid State Chem.*, 2004, **177**, 2094-2100.
31 K. M. Shaju, G. V. Subba Rao, B. V. R.Chowdari, *J. Electrochem. Soc.*, 2004, **151**, A1324-A1332.
32 J. J. Zhang, P. He, Y. Y. Xia, *J. Electroanal. Chem.*,2008, **624**, 161-166.
33 X. Y. Wang, H. Hao, J. L. Liu, T. Huang, A. S. Yu, *Electrochim. Acta*, 2011, **56**, 4065-4069.
34 Y. J. Gu,Z. Guo, H. Q. Liu, *Electrochim. Acta*, 2014, **123**, 576-581.
35 C. Ho, I. D. Raistrick, R. A. Huggins, *J. Electrochem. Soc.*, 1980, **127**, 343-350.
36 X. H. Rui, N. Ding, J. Liu, C. Li, C. H. Chen, *Electrochim. Acta*, 2010, **55**, 2384-2390.

Table of Contents

Synthesis of Novel Nitrogen-Noped Lithium Titanate with Ultra-High Rate Capability Using Melamine as A Solid Nitrogen Source

Min Guo[a], Suqing Wang[a]*, Liang-Xin Ding[a], Long Zheng[a], Haihui Wang[a,b]*

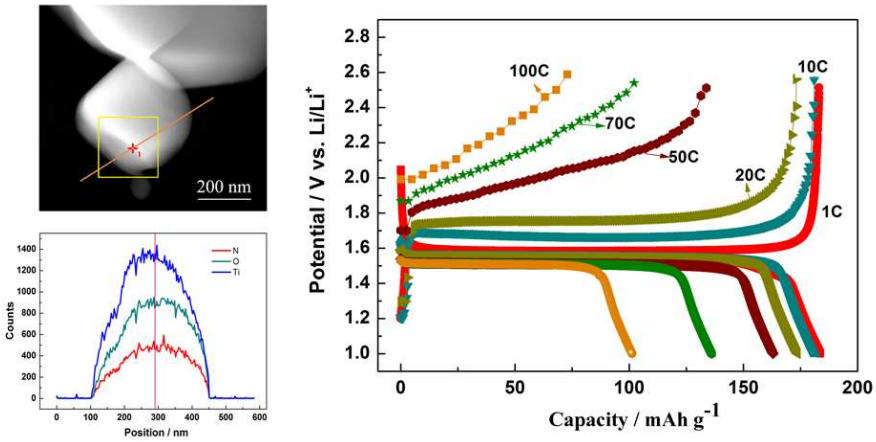

A simple and environmentally friendly route for the synthesis of N-doped $Li_4Ti_5O_{12}$ anode with excellent rate capability and cycling stability.